COBEM 2023 27TH INTERNATIONAL CONGRESS OF MECHANICAL ENGENEERING

ABCM Brazilian Society of Mechanical Sciences and Engineering
27th ABCM International Congress of Mechanical Engineering
December 04-08, 2023, Florianópolis-SC, Brazil

COBEM2023-0985
NUMERICAL INVESTIGATION OF SPLITTER PLATES AS NOISE REDUCTION TECHNIQUES FOR TANDEM CYLINDERS

Lucas Gregório Cardoso
Filipe Dutra da Silva
TEG-Thermofluids Engineering Group, Universidade Federal de Santa Catarina, Joinville, SC, Brazil
lucas.cardoso@teg.ufsc.br, filipe.dutra@teg.ufsc.br

Abstract. *In recent years, there has been an increased focus on investigating methods for aircraft noise mitigation due to demands from government regulations, created to reduce its adverse effects on the population. Tandem cylinders in cross flow represent a simplified view of some of the sound-source phenomena which occurs, for instance, in landing gears. This study addresses the area of computational aeroacoustics and aims to investigate the noise generated by vortex shedding in tandem cylinders through numerical simulations using the OpenFOAM open source code. Numerical simulations were performed for a benchmark case of a flow around a tandem cylinder model using the URANS k-ω SST turbulence model. Preliminary grid sensitivity studies considered the effects of mesh refinement in the longitudinal direction on the aeroacoustic field results, as well as the adoption of hybrid meshes that combine structured and unstructured elements. After assessing the effect of the mesh topology, the interaction of upstream cylinder vortices with the downstream cylinder surface and the effects of adding splitter plates to reduce noise for observer in the far field were studied using Ffowcs Williams-Hawkings analogy. The results showed that longitudinal mesh refinement provides accuracy for the numerical results and that adopting a hybrid mesh does not impact acoustic results, while significantly reducing processing time. Also, the addition of splitter plates was able to significantly reduce noise in the far field, attenuating spectral harmonic peaks through a mechanism that reduced the vortex shedding on the upstream cylinder, which impinge on the downstream cylinder surface, also reducing its drag coefficient.*

Keywords: *Computational aeroacoustics, airframe noise, tandem cylinders, OpenFOAM.*

1. INTRODUCTION

With the technological evolution in aviation, the market has adapted to the manufacturing and operation of aircraft with high passenger capacity in recent years, which has required that aircraft be larger and more powerful than previous ones, and therefore with more complex propulsion systems (Sanbongi, 1999). On the other hand, this technological leap has opened a range of obstacles with high noise emissions, whether due to engines or the large structures of the aircraft, leading to increased noise pollution for passengers and the population (Khardi, 2009). In order to reduce such problems, civil aviation regulatory bodies and manufacturers have joined forces to mitigate them and encourage continuous improvement. The International Civil Aviation Organization (ICAO) standardizes regulations to certify operator activities in documents such as Annex 16, which is periodically edited. Similarly, the Brazilian Civil Aviation Agency (ANAC), through the Brazilian Civil Aviation Regulation No. 36, also aims to mitigate noise in airport zones and residential areas near airports.

The noise of an aircraft can be divided into two main parts: jet noise and airframe noise. Jet noise occurs due to the interaction of flow fluctuations with the static fluid, usually present at the air outlet of turbofan and jet engines. Airframe noise, on the other hand, occurs due to the interaction of turbulent air over structures and surfaces, such as wings, fuselage, aerodynamic appendages and landing gear. The main characteristic of airframe noise is that it arises in landing situations, when engine power is reduced, and therefore there is noise pollution in residential areas near airports. Airframe noise is predominantly broadband, but can also have tonal components, and is generated by fluctuations of forces on the surfaces of complex aircraft structures (Ruijgrok, 1993).

Landing gear noise is one of the most important components of airframe noise, and is generated by the turbulent separation of flow from the structural components of the landing gear and by the interaction of the turbulence wake with downstream elements of the landing gear (Dobrzynski, 2010).

Splitter plates were chosen as noise reduction devices in this paper, as they have been widely recognized as one of the most effective passive control devices for mitigating vortex shedding downstream of a single cylinder (Kwon and Choi, 1996). Prior investigations by Gerrard (1966) have demonstrated that the Strouhal number decreases when the length L of the splitter plate is smaller than the cylinder diameter D, but increases for $D < L < 2D$. Furthermore, it has been observed that the efficiency of a splitter plate relies on both its length and the spacing between the cylinders. Notably, splitter plates longer than 2D progressively influence the drag and vortex shedding until reaching a length-to-diameter ratio of $L/D = 3$, beyond which no significant changes occur for $L/D > 3$. Moreover, for $L/D > 5$, the vortex

shedding ceases, and the drag remains constant (Apelt and West, 1975).

To delve deeper into this topic, previous numerical investigations by Bao and Tao (2013) and Abdi *et al.* (2017) explored the effects of shorter splitter plates on vortex suppression and drag reduction at low Reynolds numbers. Their findings revealed maximized effects for splitter plate angles ranging between 140 and 130°, clockwise from the stagnation point. Additionally, Duan and Wang (2021) discovered that a flexible splitter plate effectively attenuates acoustic tones by reducing fluctuations in the near-wake region of the cylinder. In the context of high Reynolds numbers, Dai *et al.* (2018) examined the influence of splitter plate width and length. They identified an optimized configuration that initially decreased turbulence kinetic energy production behind the cylinder but ultimately resulted in an increase due to the merging of the shear layers. While these aforementioned devices have been extensively discussed and documented in the literature (Cheong *et al.*, 2008; Nogueira and Carmo, 2018; Mahato *et al.*, 2019, 2021), limited attention has been given to the aerodynamic and acoustic effects in cases involving high Reynolds numbers and three-dimensional flow conditions for tandem cylinders.

To study these effects, the CFD software Open-source Field Operation and Manipulation (OpenFOAM) was used to simulate the flow around tandem cylinders. The objective of this study is to build upon the previous numerical investigation conducted by Chadlvski (2021), by introducing modifications to the Computational Fluid Dynamics (CFD) parameters, refining the simulation, adjusting the simulation time and geometry to enhance the accuracy of the results. Moreover, once the appropriate parameters for the simulation model were determined, the effectiveness of splitter plates passive noise reduction devices were evaluated. To compute the acoustic field, the Ffowcs-Williams and Hawkings (1969) acoustic analogy, implemented in the LibAcoustics library (Epikhin *et al.*, 2015), was employed.

2. METHODOLOGY

2.1 Geometry and flow conditions

The geometry and flow conditions adopted for the numerical simulation in OpenFOAM were based on the experiments conducted by Jenkins *et al.* (2005) and Lockard *et al.* (2007). Both cylinders have a diameter of $D = 0.05715$ m and a spanwise length of $16D$, with a streamwise distance of $d_{cyl} = 3.7D$ between their centers. The free-stream Reynolds and Mach numbers are $Re = 1.66 \times 10^5$ and $M = 0.1274$, respectively. Figure 1 shows the arrangement of the case, and the XYZ coordinates of microphones A, B and C are $[-8.33D, 27.815D, 8D]$, $[9.11D, 32.49D, 8D]$ and $[26.55D, 27.815D, 8D]$, respectively, with the coordinate system's origin located at the center of the upstream cylinder.

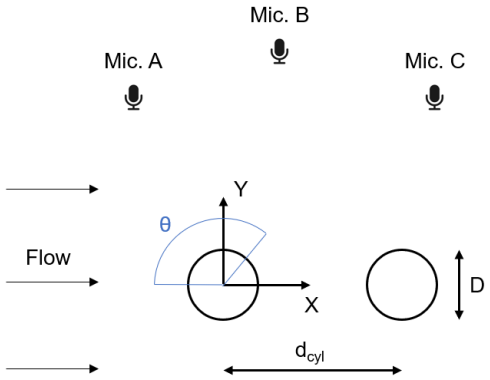

Figure 1: Arrangement of cylinders and microphones of the baseline case.

The sizing of the splitter plates on the cylinders followed the scheme presented in Figure 2, where d_{cyl}, the distance between the cylinders, is fixed at $3.7D$, L represents the length of the splitter plate, and the thickness is maintained constant at 2 mm. The flow conditions and microphone positions are the same as the baseline case (without splitter plates).

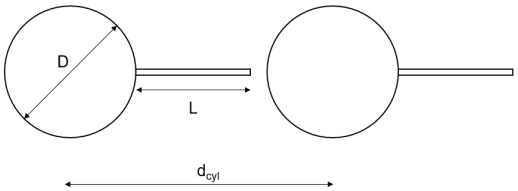

Figure 2: Parameterization of the splitter plates in the cylinders.

2.2 Flow-field simulations

The computational domain has the same dimensions as used by Chadlvski and da Silva (2021), depicted in Figure 3. The meshes were generated using the Gmsh software (Geuzaine and Remacle, 2009). The depth of the domain in the Z direction has an extension of $16D$, the same spanwise length of the cylinders in the experiments conducted by Lockard *et al.* (2007), and has a discretization of N_Z control volumes. To evaluate the three-dimensional effects of longitudinal mesh refinement, three levels of refinement, N_Z, in the Z direction were investigated in a structured mesh: 46, 69, and 103, while keeping the cell count constant on the XY plane, as shown on Table 1. This was motivated by the demonstration by Lockard *et al.* (2007) that the dependence of the aerodynamic field results on longitudinal refinement can significantly affect the acoustic field results. On the other hand, increasing the refinement leads to longer processing times.

Table 1: Number of elements of the structured baseline meshes.

Case	**Mesh**	N_Z	**Number of elements XY plane**	**Number of elements total**
Baseline	Structured	46	5.71×10^4	2.63×10^6
Baseline	Structured	69	5.71×10^4	3.94×10^6
Baseline	Structured	103	5.71×10^4	5.89×10^6

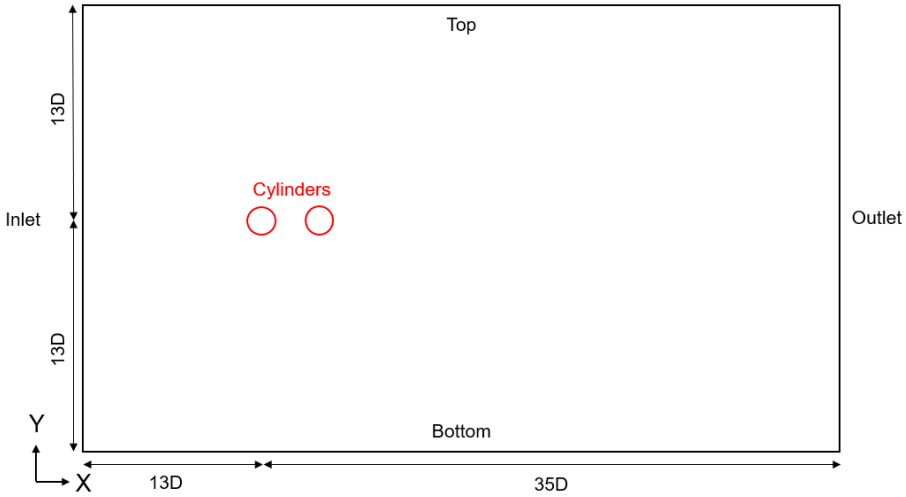

Figure 3: XY plane of the simulated computational domain with its boundaries.

In order to reduce processing time, the decision was to create three-dimensional hybrid meshes with hexahedral elements in order to ensure that the refinement yielded $y^+ < 1$ near the walls, as the accuracy of the results depends on the correct prediction of the boundary layer, while having a modest computation time. To achieve this, the mesh was generated based on mesh B from Chadlvski (2021), maintaining structured cells in the regions near the walls and in the wake downstream of the cylinders, while an unstructured mesh was employed in the remaining domain. Figure 4 presents the resulting hybrid mesh.

For the cylinders with splitter plates, the structured core follows the same refinement pattern as the baseline case in the XY plane (Figure 4). To achieve this, the same number of edge divisions and growth rates were maintained in the regions near the cylinders and in the wake. As a result, $y^+ < 1$ was ensured for both cylinders, while resulting in $1 < y^+ < 120$ on the splitter plates. Furthermore, meshes were created with variations in the length L of the splitter plate, downstream of the cylinders, in order to assess the influence of these parameters on the far-field noise. Table 2 presents the element counts for each mesh case. For instance, the case "Cylinder 1, $L = D$" signifies that a splitter plate with a length of $L = D$ is exclusively installed in the first cylinder, and this nomenclature convention applies throughout.

To solve the aerodynamic field, the OpenFOAM v2112 (OpenCFD, 2004) software was employed, using the URANS k-ω SST for turbulence model due to its computational efficiency. This modeling approach has been previous used for simulations of bluff bodies performed by the research group (da Silva *et al.*, 2020; Ribeiro *et al.*, 2021; da Silva *et al.*, 2023). Temporal discretization was performed using the Crank-Nicolson scheme with a coefficient value of 0.9. For the gradient terms, the Multi-directional cell-limited scheme with a coefficient value of 0.5 was used. For the convective terms, the second-order upwind linear scheme was used. The pressure-velocity coupling was performed through the PISO algorithm, with the Pre-Conditioned Gradient solver used for pressure computation.

The boundary conditions for pressure (p), velocity (u), turbulent kinetic energy (k) and specific turbulent kinetic energy dissipation (ω) in the OpenFOAM software are summarized in Table 3. For the near wall treatment, the kLowRe-

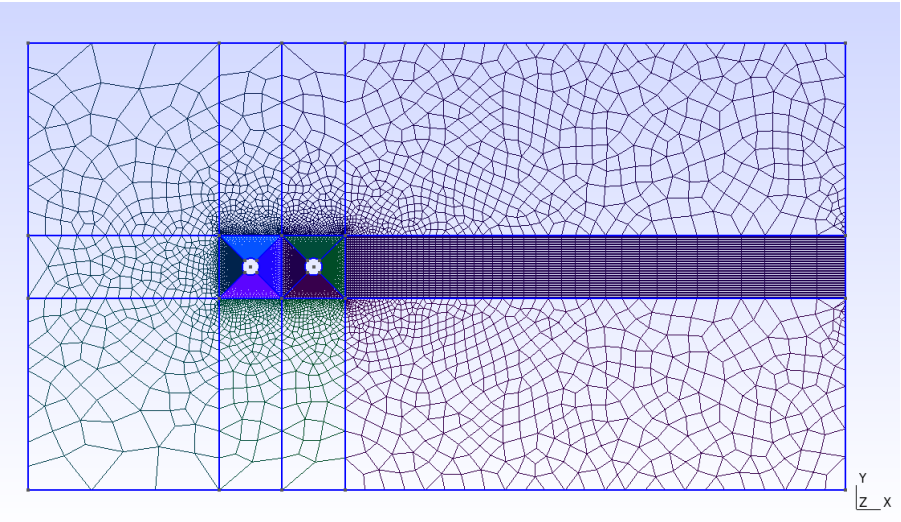

Figure 4: XY plane of computational hybrid grid of the baseline case.

Table 2: Number of elements of the mesh for each studied case.

Case	**Mesh**	N_Z	**Number of elements XY plane**	**Number of elements total**
Both, $L = D$	Hybrid	69	4.50×10^4	3.11×10^6
Cylinder 1, $L = D$	Hybrid	69	4.52×10^4	3.12×10^6
Cylinder 2, $L = D$	Hybrid	69	4.52×10^4	3.12×10^6
Both, $L = 2D$	Hybrid	69	4.24×10^4	2.93×10^6
Cylinder 1, $L = 2D$	Hybrid	69	4.26×10^4	2.94×10^6
Cylinder 2, $L = 2D$	Hybrid	69	4.26×10^4	2.94×10^6
Baseline	Hybrid	69	4.64×10^4	3.20×10^6

WallFunction was used, which adjusts the model settings (low Reynolds approach or wall function) based on the y^+ value of the mesh. This approach, as described by Liu (2016), was chosen to account for both the high resolution of the grid near the cylinders and the lower resolution of the regions adjacent to the splitter plates. The magnitude of the turbulent kinetic energy was determined using a turbulent intensity of $I = 0.1\%$, as indicated by the experiments conducted by Jenkins *et al.* (2005), and an eddy viscosity ratio of $\nu_t/\nu = 2$ (Chadlvski and da Silva, 2021).

Table 3: Boundary conditions for the simulation.

Boundary	**Pressure**	**Velocity**	**Turbulent kinetic energy**	**Specific turbulent kinetic energy dissipation**
Inlet	freeStream (0 Pa)	freeStream (44 m/s)	freeStream (0.00325 m²/s²)	freeStream (43 1/s)
Outlet	fixedValue (0 Pa)	zeroGradient	zeroGradient	zeroGradient
Front and back	zeroGradient	slip	zeroGradient	zeroGradient
Top and bottom	freeStream (0 Pa)	freeStream (44 m/s)	freeStream (0.00325 m²/s²)	freeStream (43 1/s)
Cylinders	zeroGradient	noSlip	kLowReWallFunction	omegaWallFunction

To satisfy the Courant condition ($Co < 1$), the nondimensional time step Δt_{step} for all simulations was chosen as $\Delta t_{step} U_0/D = 3.08 \times 10^{-3}$. To ensure a statistically stationary regime, the sampling time Δt_{sample} was established as $\Delta t_{sample} U_0/D = 323$. Parallel processing was employed for the simulations on the computer cluster of the Laboratory of Scientific Computing (LabCC) at UFSC - CTJ.

2.3 Far-field noise computation

Prediction of far-field noise was performed based on Ffowcs-Williams and Hawkings (1969) (FW-H) analogy, available in the LibAcoustics library (Epikhin *et al.*, 2015). Since the FW-H analogy requires permeable surfaces around the cylinders to store the pressure and velocity data, surface 4 created by Chadlvski and da Silva (2021) was used with a minor modification: the distance between the upper and lower face boundaries was changed from $2.5D$ to $1.85D$ to include the entire surface in the structured region of the mesh. The image of the FW-H surface in red, overlaid on the mesh, can be visualized in Figure 5.

Once the pressure values were calculated using the analogy, to obtain the acoustic pressure spectrum as a function of frequency, the power spectral density (PSD) of the acoustic pressure was calculated in dB/Hz using a Python algorithm with a frequency resolution of 12.5 Hz and applying the method proposed by Welch (1967). The signal was segmented into blocks and subjected to Fast Fourier Transform (FFT), using the Hanning window, with a 75% overlap between each block.

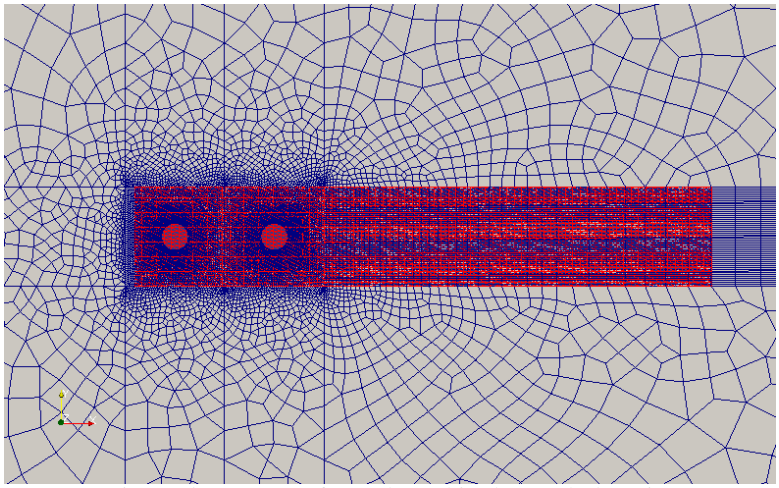

Figure 5: FW-H surface adopted in the mesh domain.

3. RESULTS

In this section, the results obtained by the numerical model in OpenFOAM and LibAcoustics are presented and discussed. First, a comparison is made between the experimental results and the numerical results of the structured baseline mesh, with different levels of refinement in the Z-direction. Furthermore, a comparison between the structured and hybrid meshes is conducted, considering the accuracy of the results and the computational cost. Finally, the parametrization of the simple splitter plates is evaluated in terms of the reduction of far-field noise.

3.1 Baseline case

In Figure 6, it can be noted that the numerical solution was able to satisfactorily predict the frequencies of the second and third peaks for microphones A (Figure 6a), B (Figure 6b), respectively, although with some errors in their magnitude. The predicted peak levels were notably elevated, likely attributed to limitations in the URANS k-ω SST turbulence model. The results obtained for $N_Z = 69$ and $N_Z = 103$ show a high similarity, although the latter had a processing time 56% higher. For a proper comparison of the tonal noise level, the numerical PSD shown in Figure 6 was corrected to account for the different frequency bandwidth between the numerical results and experimental data from Lockard *et al.* (2007).

To save computational processing time, the study proceeded with the comparison between structured and hybrid meshes with $N_Z = 69$. For the hybrid mesh, it can be observed in Figure 7 that for all three microphones, the frequencies of the spectral peaks are identical in both studied meshes, while having a 44% processing time reduction. In the first peak, the power spectral densities (PSD) are equal for both meshes, while in the second and third peaks, the value for the hybrid mesh is slightly higher than that of the structured mesh. The maximum difference between these peaks was 3.5 dB/Hz, occurring in the second peak for microphone A (Figure 7a).

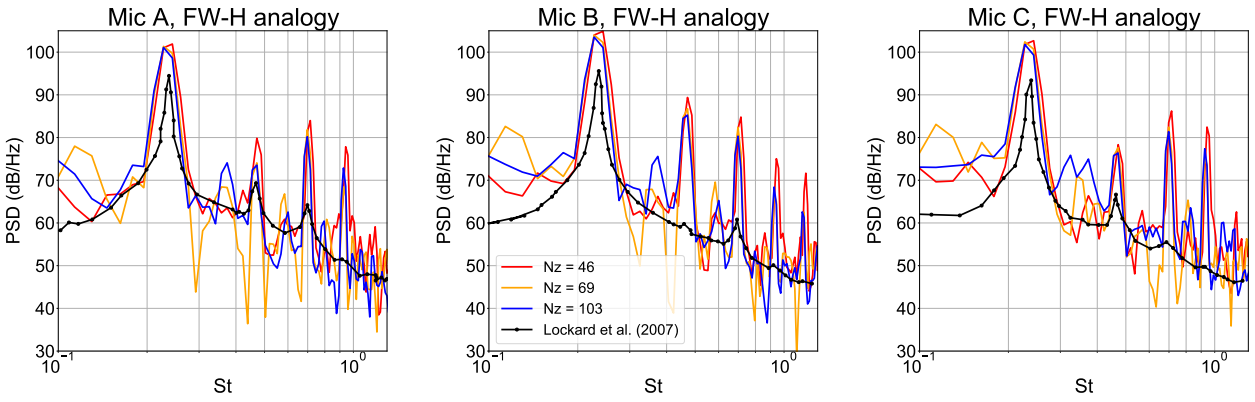

(a) (b) (c)

Figure 6: Comparison of the PSD spectra obtained from different structured mesh longitudinal refinements, for microphones A, B and C.

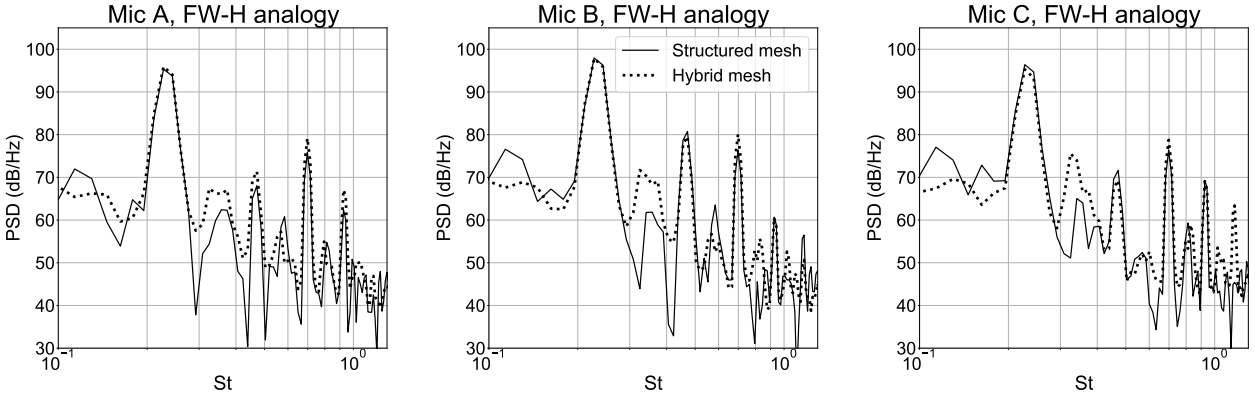

(a) (b) (c)

Figure 7: Comparison of the PSD spectra obtained from structured and hybrid meshes, $N_Z = 69$, for microphones A, B and C.

The evolution of the flow and the behavior of the vortices in the cylinders can be observed in Figure 8, which shows the magnitude of the velocity with a time interval of $\Delta t U_0/D = 11.54$.

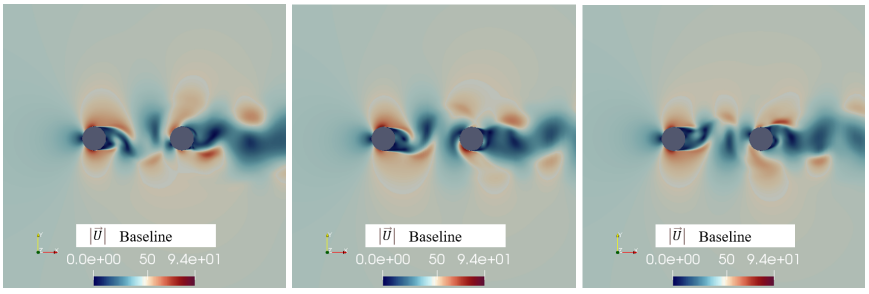

(a) t_0 (b) $t_0 + 11.54\frac{D}{U_0}$ (c) $t_0 + 23.08\frac{D}{U_0}$

Figure 8: Evolution of the flow for the baseline case.

3.2 Effects of the use of splitter plates

Comparative studies were conducted using the hybrid mesh with splitter plates on both cylinders, as well as on only one of the cylinders, in comparison to the baseline case without any splitter plates. Each line in the graphs represents a distinct configuration. The far-field noise results presented generally indicate a reduction in the magnitude of the peaks for all three microphones compared to the baseline case.

Comparing the acoustic results between the two dimensions of the splitter plate on both cylinders, $L = D$ and $L = 2D$, Figure 9 shows that increasing the plate length resulted in a greater reduction in spectral noise, which attenuated the $St \approx 0.32$ peak by approximately 25 dB/Hz and showed lower PSD values across the entire spectrum, especially at higher frequencies. Also, Figure 10 shows the attenuation of the vortices on the upstream cylinder and the flow attachment on the spliter plate.

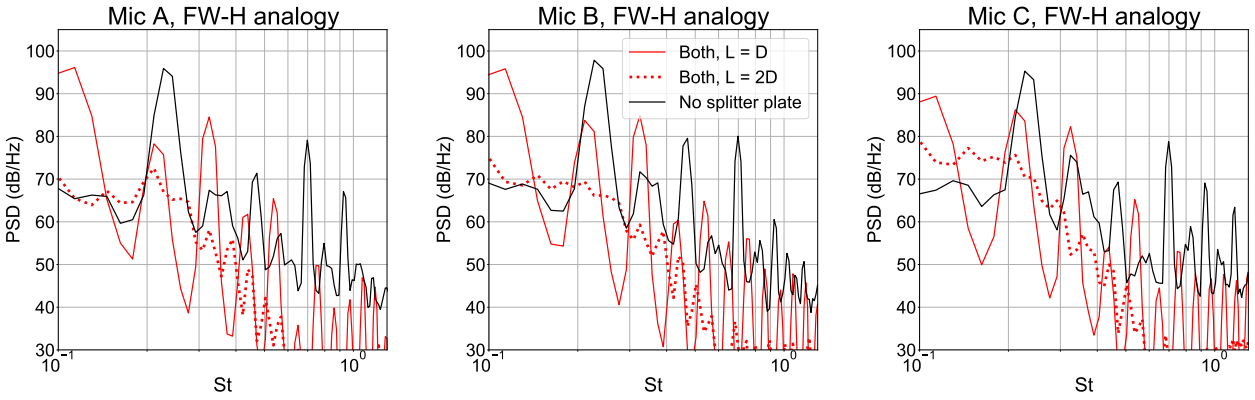

(a) (b) (c)

Figure 9: Comparison of the PSD spectra obtained with $L = D$ and $L = 2D$ on both cylinders, for microphones A, B and C.

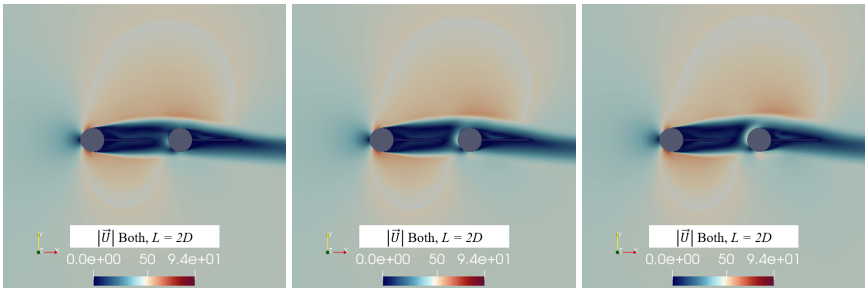

(a) t_0 (b) $t_0 + 11.54\frac{D}{U_0}$ (c) $t_0 + 23.08\frac{D}{U_0}$

Figure 10: Evolution of the flow for the case "Both, $L = 2D$".

On the other hand, in the configuration with the splitter plate only on the first cylinder (Figure 11), the spectral density values are close in the range of $0.2 < St < 0.3$, decreasing as the frequency increases for a plate length of $L = 2D$. It was possible to perceive the attenuation of the vortices in the region of $\theta = 45°$ of cylinder 2, caused by the presence of the splitter plate in the first cylinder, in Figure 12.

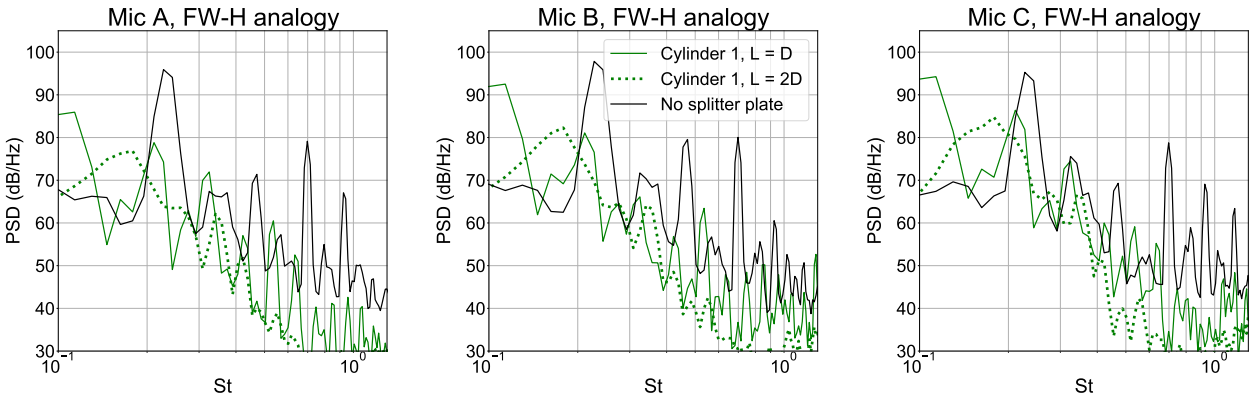

(a) (b) (c)

Figure 11: Comparison of the PSD spectra obtained with $L = D$ and $L = 2D$ on cylinder 1, for microphones A, B and C.

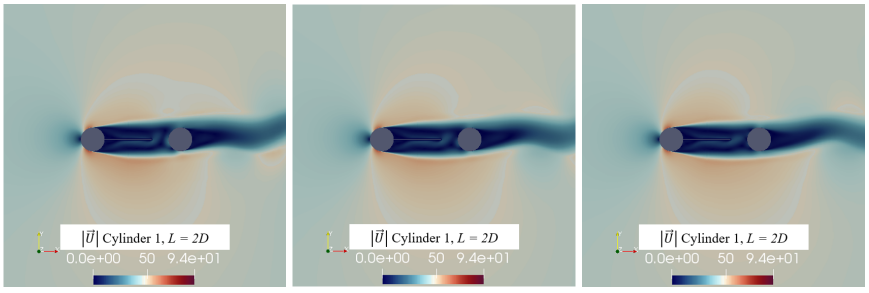

(a) t_0 (b) $t_0 + 11.54\frac{D}{U_0}$ (c) $t_0 + 23.08\frac{D}{U_0}$

Figure 12: Evolution of the flow for the case "Cylinder 1, $L = 2D$".

Figure 13 demonstrates that the addition of the splitter plate only on the second cylinder resulted in the emergence of a peak near the vortex shedding frequency (first peak at $St \approx 0.26$), with a magnitude similar to the case without the splitter plate, as well as peaks at higher frequencies but with slightly lower PSD magnitudes. Furthermore, a shift towards lower frequencies in the noise spectrum was observed. There was no significant vortex attenuation on downstream cylinder, as shown in Figure 14.

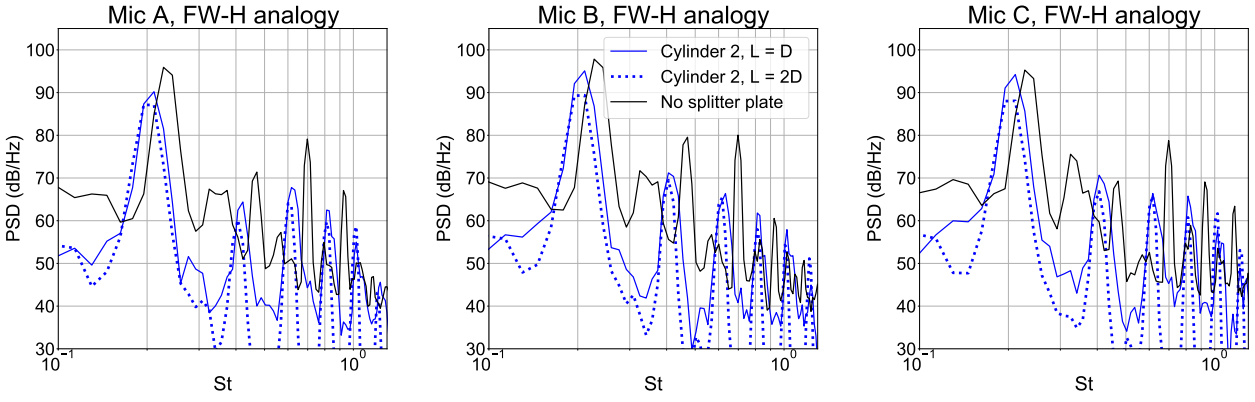

(a) (b) (c)

Figure 13: Comparison of the PSD spectra obtained with $L = D$ and $L = 2D$ on cylinder 2, for microphones A, B and C.

The drag reduction, as shown in Table 4, was significant for the case where the plate dimension is equal to $2D$, mainly due to the increase in plate dimension up to a value close to the length of the recirculation bubble (Kwon and Choi, 1996). Furthermore, it was observed that the results obtained for configurations with plates on both cylinders and only on cylinder 1 were similar for the upstream cylinder, suggesting that a large part of the drag reduction of the system is due to

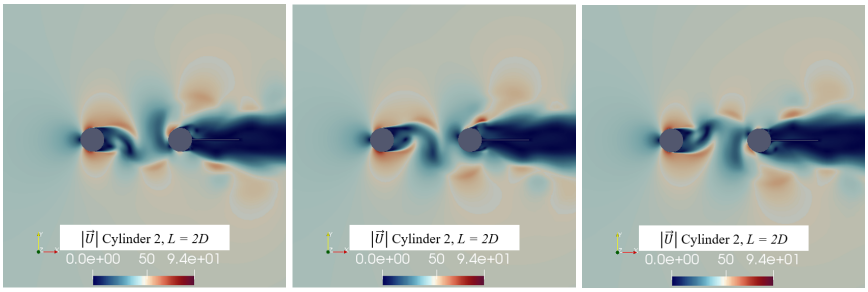

(a) t_0 (b) $t_0 + 11.54\frac{D}{U_0}$ (c) $t_0 + 23.08\frac{D}{U_0}$

Figure 14: Evolution of the flow for the case "Cylinder 2, $L = 2D$".

the presence of the plate on the upstream cylinder. In the case of the splitter plate only on cylinder 2, there was only drag reduction on that cylinder.

Table 4: Average drag coefficient for the studied cases.

	$\bar{C}_{d1}$		$\bar{C}_{d2}$	
Case	$L = D$	$L = 2D$	$L = D$	$L = 2D$
Both	0.569	0.549	0.098	0.054
Cylinder 1	0.563	0.546	0.180	0.057
Cylinder 2	0.788	0.753	0.253	0.277
Baseline	0.684		0.354	

4. CONCLUSION

The study of the baseline case revealed that increasing the mesh refinement level in the longitudinal direction of the cylinders had different impacts on the various analyzed quantities. For the acoustic field, the mesh with refinement $N_Z = 69$ yielded results similar to those with refinement $N_Z = 103$, particularly in the spectral peaks, but with a 56% lower processing time. The adoption of a hybrid mesh, which combines structured elements in the flow region near the cylinders and unstructured elements in distant regions, proved to be an effective strategy for optimizing computational time, reducing it by 44% compared to the structured mesh, without compromising the accuracy of the acoustic results.

The insertion of splitter plates with length $L = D$ in the cylinders resulted in a reduction of acoustic peaks for FW-H analogy. The insertion of the splitter plate in the first cylinder mitigated vortex generation on the surface of the second cylinder, reducing the acoustic peaks in the spectrum. On the other hand, the insertion of the splitter plate only in the downstream cylinder had little effect on noise reduction, maintaining peaks with slightly lower magnitudes than in the baseline case. For the splitter plate with length $L = 2D$, the effects were even more noticeable. The plate was able to significantly reduce the vortices originated in the upstream cylinder, suppressing pressure fluctuations in the second cylinder. This mechanism led to a attenuation of the noise spectrum peaks for both cases in which the plate was inserted in the first cylinder. For the plate inserted only in the second cylinder, there was again a slight attenuation in the peaks, but with a shift to lower frequencies.

Finally, the splitter plate decreased the average drag coefficient for both cylinders, as the length increased on cases with the splitter plate on the upstream cylinder. On the other hand, the insertion of the splitter plate only on the downstream cylinder had less effect on drag reduction.

5. REFERENCES

Abdi, R., Rezazadeh, N. and Abdi, M., 2017. "Reduction of fluid forces and vortex shedding frequency of a circular cylinder using rigid splitter plates". *European Journal of Computational Mechanics*, Vol. 26, No. 3, pp. 225–244.

Apelt, C. and West, G., 1975. "The effects of wake splitter plates on bluff-body flow in the range $10^4 < Re < 5 \times 10^4$, Part 2". *Journal of Fluid Mechanics*, Vol. 71, No. 1, pp. 145–160.

Bao, Y. and Tao, J., 2013. "The passive control of wake flow behind a circular cylinder by parallel dual plates". *Journal of Fluids and Structures*, Vol. 37, No. 1, pp. 201–219.

Chadlvski, J.V.V.M., 2021. "Análise e validação de modelo de simulação numérica para previsão de ruído aerodinâmico utilizando openfoam e libacoustics". Joinville, p. 1-76.

Chadlvski, J.V.V.M. and da Silva, F.D., 2021. "Prediction of aerodynamic noise generated by cylinders in uniform flow using OpenFOAM". International Congress of Mechanical Engineering.

Cheong, C., Joseph, P., Park, Y. and Lee, S., 2008. "Computation of aeolian tone from a circular cylinder using source models". *Applied Acoustics*, Vol. 69, No. 2, pp. 110–126.

da Silva, F.D., de Bittencourt Ribeiro, E., Silva, E. and Tancredi, T.P., 2020. "Prediction of drag on submarines using openfoam". In *18th Brazilian Congress of Thermal Sciences and Engineering*. Brazilian Association of Engineering and Mechanical Sciences. doi:10.26678/ABCM.ENCIT2020.CIT20-0513.

da Silva, F.D., Tancredi, T.P. and Silva, E., 2023. "Corrections for the drag on submarines due to the blockage effect". *Ocean Engineering*, Vol. 275, p. 114150. ISSN 0029-8018. doi:https://doi.org/10.1016/j.oceaneng.2023.114150.

Dai, S., Younis, B.A., Zhang, H. and Guo, C., 2018. "Prediction of vortex shedding suppression from circular cylinders at high reynolds number using base splitter plates". *Journal of Wind Engineering and Industrial Aerodynamics*, Vol. 182, No. 1, pp. 115–127.

Dobrzynski, W., 2010. "Almost 40 years of airframe noise research: what did we achieve?" *Journal of aircraft*, Vol. 47, No. 2, pp. 353–367.

Duan, F. and Wang, J., 2021. "Fluid–structure–sound interaction in noise reduction of a circular cylinder with flexible splitter plate". *Journal of Fluid Mechanics*, Vol. 920, p. A6.

Epikhin, A., Evdokimov, I., Kraposhin, M., Kalugin, M. and Strijhak, S., 2015. "Development of a dynamic library for computational aeroacoustics applications using the openfoam open source package". *Procedia Computer Science*, Vol. 66, No. 1, pp. 150–157.

Ffowcs-Williams, J.E. and Hawkings, D.L., 1969. "Sound generation by turbulence and surfaces in arbitrary motion". *Philosophical Transactions of the Royal Society of London. Series A, Mathematical and Physical Sciences*, Vol. 264, No. 1151, pp. 321–342.

Gerrard, J., 1966. "The mechanics of the formation region of vortices behind bluff bodies". *Journal of fluid mechanics*, Vol. 25, No. 2, pp. 401–413.

Geuzaine, C. and Remacle, J.F., 2009. "Gmsh: A 3-d finite element mesh generator with built-in pre-and post-processing facilities". *International journal for numerical methods in engineering*, Vol. 79, No. 11, pp. 1309–1331.

Jenkins, L., Khorrami, M., Choudhari, M. and McGinley, C., 2005. "Characterization of unsteady flow structures around tandem cylinders for component interaction studies in airframe noise". In *11th AIAA/CEAS aeroacoustics conference*. p. 2812.

Khardi, S., 2009. "Reduction of commercial aircraft noise emission around airports. a new environmental challenge". *European Transport Research Review*, Vol. 1, No. 4, pp. 175–184.

Kwon, K. and Choi, H., 1996. "Control of laminar vortex shedding behind a circular cylinder using splitter plates". *Physics of Fluids*, Vol. 8, No. 2, pp. 479–486.

Liu, F., 2016. "A thorough description of how wall functions are implemented in openfoam". *Proceedings of CFD with OpenSource Software*, Vol. 34.

Lockard, D., Khorrami, M., Choudhari, M., Hutcheson, F., Brooks, T. and Stead, D., 2007. "Tandem cylinder noise predictions". In *13th AIAA/CEAS Aeroacoustics Conference (28th AIAA Aeroacoustics Conference)*. p. 3450.

Mahato, B., Ganta, N. and Bhumkar, Y.G., 2019. "Control of aeroacoustic noise generation during flow past a circular cylinder using splitter plate". In *INTER-NOISE and NOISE-CON Congress and Conference Proceedings*. Institute of Noise Control Engineering, Vol. 259, pp. 3839–3848.

Mahato, B., Ganta, N. and Bhumkar, Y.G., 2021. "Effective control of aeolian tone using a pair of splitter plates". *Journal of Sound and Vibration*, Vol. 494, No. 1, pp. 115906 – 115906.

Nogueira, L.W. and Carmo, B.S., 2018. "Numerical analysis and acoustic optimization of a detached splitter plate applied for passive cylinder wake control". *Journal of the Brazilian Society of Mechanical Sciences and Engineering*, Vol. 40, No. 1, p. 37. ISSN 1806-3691. doi:10.1007/s40430-017-0931-5. URL `https://doi.org/10.1007/s40430-017-0931-5`.

OpenCFD, 2004. "Openfoam programmer's guide".

Ribeiro, E.d.B., Tancredi, T.P., da Silva, F.D. and Silva, E., 2021. "Comparison between axisymmetric and 3d models for the evaluation of drag on submarine hulls". In *26th International Congress of Mechanical Engineering*. Brazilian Association of Engineering and Mechanical Sciences. doi:10.26678/ABCM.COBEM2021.COB2021-0409.

Ruijgrok, G.J., 1993. *Elements of aviation acoustics*. Delft University Press, Delft, 1st edition.

Sanbongi, B., 1999. "The aircraft engine: An historical perspective of engine development through World War I". *Journal of Aviation/Aerospace Education & Research*, Vol. 8, No. 3, pp. 7–17.

Welch, P., 1967. "The use of fast fourier transform for the estimation of power spectra: a method based on time averaging over short, modified periodograms". *IEEE Transactions on audio and electroacoustics*, Vol. 15, No. 2, pp. 70–73.

6. RESPONSIBILITY NOTICE

The authors are solely responsible for the printed material included in this paper.